Gelenbe, E., & Kocak, T. (2000). Area-based results for mine detection. IEEE Transactions on Geoscience and Remote Sensing, 38(1), 12 - 24. 10.1109/36.823897

Area-Based Results for Mine Detection

Erol Gelenbe, *Fellow, IEEE,* and Taşak Koçak, *Member, IEEE*

***Abstract*—The cost and the closely related length of time spent in searching for mines or unexploded ordnance (UXO) may well be largely determined by the number of false alarms. False alarms can result in time consuming digging of soil or in additional multisensory tests in the minefield. In this paper, we consider two area-based methods for reducing false alarms. These are: a) the previously known "declaration" technique [8], [10] and b) the new δ technique, which we introduce. We first derive expressions and lower bounds for false-alarm probabilities as a function of declaration area and discuss their impact on receiver operation characteristic (ROC) curves. Second, we exploit characteristics of the statistical distribution of sensory energy in the immediate neighborhood of targets and of false alarms from available calibrated data, to propose the δ technique, which significantly improves discrimination between targets and false alarms. The results are abundantly illustrated with statistical data and ROC curves using electromagnetic-induction sensor data made available through DARPA [8] from measurements at various calibrated sites.**

***Index Terms*—Area-based techniques for detection, declaration, δ technique, detection of unexploded ordinance (UXO), electromagnetic induction sensors, mine detection.**

I. Introduction

AUTOMATIC mine detection and the detection of unexploded ordnance have become a subject of great importance, and a variety of sensors and processing systems have been proposed recently for mine remediation. A number of novel technical approaches to this major problem have emerged based on a variety of sensor technologies [9], [11]–[15], and the field is now on the verge of significant scientific and technical development. All approaches are based on the on-line or off-line algorithmic processing of data from single or multiple sensors and on data-fusion techniques that can take advantage of the complementary characteristics of different sensors. In this framework, availability of multisensory data [8] from calibrated minefields (and from minefields that offer significant challenge to detection algorithms) are particularly useful.

In remedial mine detection, which is primarily directed toward an exhaustive removal of mines for humanitarian purposes, both the probability of correct detection of a mine and the probability of false alarm, are important performance metrics for any sensor or processing algorithm. The probability of detection is important for obvious reasons. However, the probability of false alarm is also of major importance for simple reasons of cost. The number of false alarms is bound to be significantly greater than the number of mines found in a given area. Hence, the cost and the closely related duration of the search for mines may well be largely determined by the large number of false alarms that will lead to unnecessary and time consuming digging of soil in the minefield. Thus, all sensors and algorithms need to address these important metrics.

There have been several studies of mine detection using statistical methods and involving different sensors, including [1]–[7], [12], [14]–[19]. In the case of the direct point-by-point exhaustive detection and search for mines, which is directly related to the present work, current detection techniques do not provide sufficiently high performance results, especially in cases where the minefield is heavily cluttered [9], [10]. Indeed, it can be expected that clutter will be prevalent in many minefield environments, since the same areas will have been used by troops in the field (littering the area with cans or spent cartridges), or simply because the minefields of interest in remedial demining may be located in populated areas. Similarly, areas that contain a lot of unexploded ordnance, such as firing ranges on or close to military bases, will contain a variety of metallic objects or other clutter which results from long term human presence. Thus, most technologies in use or that have been proposed for detecting land mine and unexploded ordnance (UXO) will typically lead to high false-alarm rates, even at relatively low probabilities of correct detection [8], [10]. Thus, the objective of this research is to develop technologies that provide accurate detection of mines in cluttered environments, with acceptably low false-alarm rates.

In order to summarize the basic concepts related to mine detection, it may be helpful to consider the summary representation of Table I. We see that if a mine exists at some location, the detector that visits that location will either correctly detect it or will miss it. On the other hand, if a mine does not exist at the location being examined, either the detector will incorrectly detect a mine yielding a false alarm, or it will correctly indicate that it does not exist.

The minefield data we will use in this study is based on measurements provided by DARPA [8], with two different electromagnetic-induction sensor systems at a variety of geographic locations. This data has been collected in a series of systematic minefield-sensing experiments, which have been conducted at multiple locations with a variety of sensors and implanted with decoy mines and mine-like objects. The first sensing system considered is a Geonics EM61-3D three-component, time-domain sensor. It consists of a multichannel pulsed-induction system, having a 1-m square transmitter coil and three orthogonal 0.5-m receiver coils, which are positioned approximately 0.3 m above the ground. The second system consists of a 0.5 m Geonics EM61 pulsed-induction sensor equipped with two

Manuscript received August 26, 1997; revised July 13, 1998. This work was supported in part by the MURI on Demining, under U.S. Army Research Office Grant DAAH04-96-1-0448.

E. Gelenbe is with the School of Electrical Engineering and Computer Science, University of Central Florida, Orlando, FL 32816 USA (erol@cs.ucf.edu).

T. Koçak is with Mitsubishi Semiconductor America, Durham, NC 27704 USA (e-mail: tkocak@ee.duke.edu).

Publisher Item Identifier S 0196-2892(00)00003-6.

TABLE I
DIFFERENT EVENTS RELATED TO MINE DETECTION

Buried Mine	Detected?	Result
EXISTS	YES	CORRECT DETECTION
EXISTS	NO	MISSED TARGET
DOES NOT EXIST	YES	FALSE ALARM
DOES NOT EXIST	NO	CORRECT NON-DETECTION

coplanar 0.5-m coils with a vertical spacing of 0.4 m. The sensor height above ground level is again approximately 0.3 m. Specifically, the data we will use represents the measurements collected in a roughly 100 × 100 square-meter area for four different regions. In order to be consistent with data description, we will use the following names for these regions, which will prove to have significantly different clutter characteristics, as well as different target (decoy mine) locations. They will refer to them as firing point (FP) 20, firing point (FP) 22, Seabee, and Turkey Creek. An example of EMI energy data is shown on Fig. 1 for 1-m Z-Coil measurements obtained by DARPA [8]. The vertical lines simply indicate target locations and do not represent energy values. The area that appears to have zero energy is simply an area for which we do not have any data (e.g., it may not have been surveyed). Inspection of the figure shows the significant amount of clutter in various areas and the relatively low energy levels at target locations.

The EMI energy level we use is a derived quantity from DARPA's raw data.

1) For 1-m data, the Geonics EM61-3D sensor data was collected along survey lines spaced 1 m apart in the east direction and at a rate of three samples per second, or at approximately 0.4-m intervals in the north direction. For each measurement point, the instrument's output is measured and recorded at 20 geometrically spaced time gates covering a time range from 320 μs to 32 ms. The energy level we use for each point is derived as follows:

$$E = \sum_{i=1}^{20} X^2(i) \tag{1}$$

where $X(i)$ is the EM61-3D sensor output for the ith time interval.
2) The 0.5-m data was collected along survey lines spaced at 0.5-m intervals in the east direction and 0.2-m intervals in the north direction. For this data, the received signal's absolute value from the Geonics EM61 is integrated from 0.18 to 0.87 ms after each transmit pulse, resulting in a single data point Y for each location. The energy level for each point is then simply obtained as $E = Y^2$.
3) Because of the relative inaccuracy of the position measurements, the minefields considered are artificially gridded on the basis of 1 m × 1 m blocks. All the energy data is then mapped by averaging it onto this grid. Specifically, for both the 1-m and 0.5-m data, the energy values are averaged on the 1 m × 1 m block, which contains the points where the values are measured.

As mentioned earlier, a source of inaccuracy in the practical use of the data we employ in this study is related to the exact location of the sensor being used as data was registered. This is due to a variety of instrumentation and data-collection effects, leading to errors in registering the sensor's position as it travels continuously across the minefield. Hence, we have followed a commonly accepted procedure suggested for using this data, which is to register the mine locations by analyzing the energy levels near the approximate known mine locations. We assume that if there is a mine at a particular point, then its immediate neighbors should have lower energies. To give an idea of this effect, two of the 5 m × 5 m regions that we examine are shown in Fig. 2.

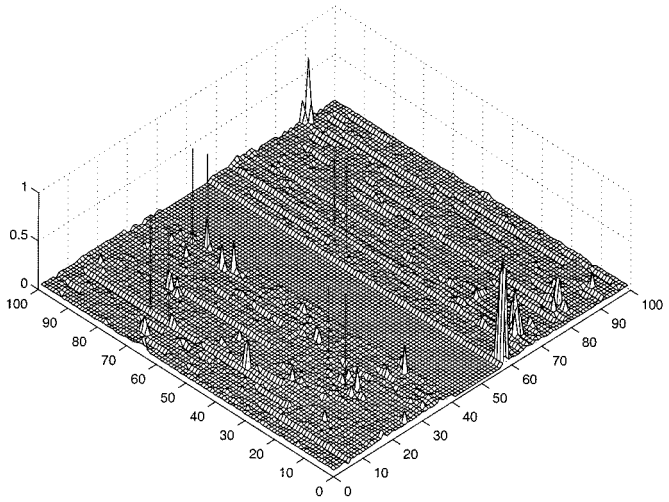

Fig. 1. Relative energy values measured at FP 20 site at 1 m resolution from the Z coil of the Geonics EM61-3D sensor. Vertical lines show some mine positions, illustrating the difficulty of detecting mines directly from measured energy.

II. EFFECT OF "DECLARATION" ON FALSE ALARMS AND ROC

An established practice [8], [10] in processing minefield data is the so-called process of "declaration," which is based on the simple remark that whenever a false alarm or a mine is detected (i.e., whenever the sensor and detection algorithm says "alarm"), an *area at and around* the position at which the signal was detected is thoroughly searched. This search will typically involve visual inspection and perhaps digging with specialized tools and probes, but also will often entail the use of other sensors. Thus, when an alarm occurs, an area that includes that point is thoroughly checked out and all mines are found or no mines are found (i.e., it was a false alarm). It is convenient to simplify the area explored as being an $h \times h$ area centered at the point at which the detection occurred, where h is in an appropriate unit (e.g., in meters).

h is taken to be an odd integer, so that the center point of the area is the location of detection. Because of the important effect declaration has on false-alarm rates, in this section, we derive some bounds on false-alarm probabilities with declaration as compared to false-alarm probabilities obtained without declaration.

In practice, the choice of h will depend on the search procedure being followed in the field. Thus, several authors [10], [12] present ROC curves for different sensors and processing

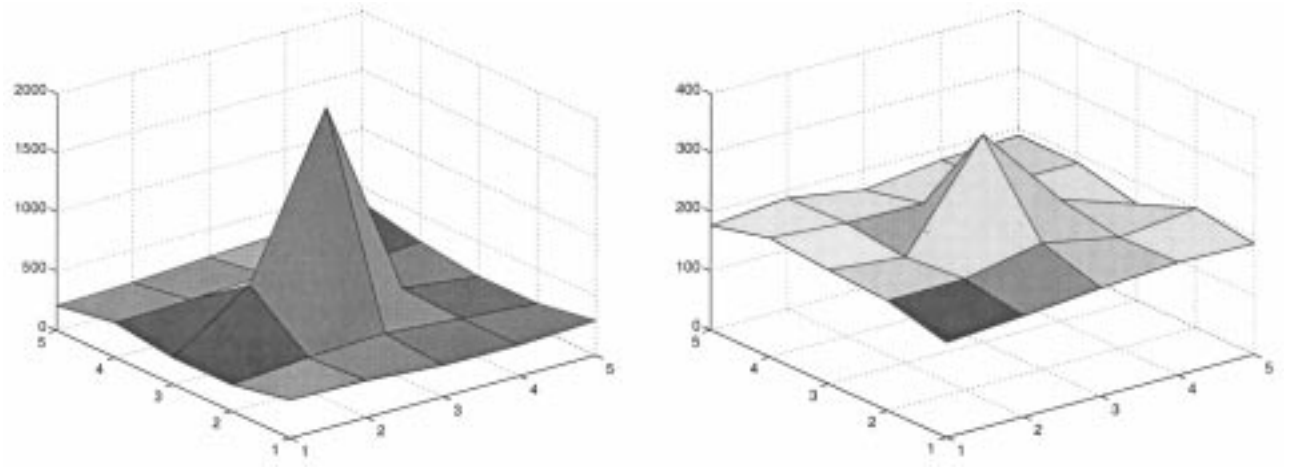

Fig. 2. Energy profiles at two mine locations in the FP 20 site (left) and the Turkey Creek site (right). The Y-axis shows the measured Z-coil energy values.

algorithms for a range of values of h varying between $h = 1$ (when the declaration procedure is simply not being used) to $h = 3, 5, 7$. Notice that a 49-m^2 area may be considered to be excessively large for a search around a presumed mine when the unit is in meters. However, when we are dealing with half-meter grids for the minefield, an approximately 12-m^2 search area corresponding to $h = 7$ might be a reasonable value to consider.

Whenever a mine or a false alarm is located at some point p, the $h \times h$ set of points $A_h(p)$ centered at p will be considered to have been explored and will be removed from further consideration concerning false-alarm rates. By "point" p, we mean some location $p = (x, y)$ in the minefield, assuming that the whole field has been discretized in 1×1 unit squares, so that point (0, 0) would in fact refer to the square contained in the vertices (0, 0), (0, 1), (1, 0), (1, 1). Note that if some point $q \in A_h(p)$ has been included previously in the declaration area of some other point p' where a mine or false alarm has previously been detected, then q should not be eliminated twice from the areas being scanned. In general though, it is of interest to have a theoretical understanding of how the procedure of declaration affects ROC curves. However, the precise effect of h on the ROC curves is particularly difficult to determine theoretically, since it depends on the distribution of mines and of false alarms in the field, and especially on their proximity to each other. An exact computation of the effect of h would have to make assumptions about the spatial statistics of targets and false alarms, and would therefore be poor estimates of the results obtained with real data. Therefore, in this section we derive robust bounds, which do not depend on statistical assumptions or on the nature of a particular minefield, for the impact that h will have on the probability of false alarm and the probability of correct detection.

Let us first develop some notation. Consider a minefield in which the mine locations are denoted by the set T, while the nonmine points where the detector may declare a false alarm (i.e., those points where the energy response to a sensor is nonzero) are denoted by the set N. We write $S = T \cup N$ and $|T|$, $|N|$, $|S|$ will be the sizes of the sets. Let $P_{f1}(h)$, $P_{d1}(h)$ be the probability of false alarm and the probability of correct detection, respectively, when a declaration area of size $h \times h$ is used. For $h = 1$ (i.e., with no declaration, these will be denoted P_f, P_d). Typically, we will have $|N| \gg |T|$ (i.e., we may have thousands of nonmine points in a minefield, with perhaps 10 or 20 mines). Ratios may be somewhat different if the targets sought are unexploded ordnance (UXO), but the $|N|$ would still be much larger than $|T|$. The following results are only valid for sensors or detectors that use point data and base their decisions concerning the presence or absence of a mine or of a false alarm at a given point p on sensor output [call it $E(p)$] at that single point p, rather than at its surroundings or in other areas. This differs from some of the algorithms that will be discussed later in this paper. Note that the following results refer to any given run of a detection algorithm on measured data on a specific minefield. Thus, the probabilities $P_{f1}(h)$, $P_{d1}(h)$ are simply the ratio of measured numbers

$$P_{f1}(h) = \frac{F(h)}{|N|}, \tag{2}$$

$$P_{d1}(h) = \frac{D(h)}{|T|} \tag{3}$$

where $F(h)$ is the number of false alarms, and $D(h)$ is the number of correct detections counted with a declaration area of $h \times h$. All the following results concerning declaration (Propositions 1–3) assume that the false-alarm rate P_f with $h = 1$ is homogeneous for all points p in the minefield data. Our first result is

Proposition 1: Consider a detector that only uses sensor data measured at a point p to make decisions about that same point. Let $P_{f1}(h)$ be the false-alarm rate with an $h \times h$ declaration area. Then a lower bound for $P_{f1}(h)$ for any (odd-valued) h is given by

$$P_{f1}(h) \geq \frac{P_f - \dfrac{|T|}{|N|} P_{d1}(h)(h^2 - 1)}{1 + P_f(h^2 - 1)}. \tag{4}$$

Comment: The total number of false alarms in the detection procedure is $F(h) = P_{f1}(h).|N|$, and for $h = 1$, we write $F = P_f.|N|$. $P_{f1}(h)$ can be empirically determined as the number of 1 m $\times$ 1 m grid points where false alarms are detected in the whole minefield, divided by the total area size of the mine field,

when a declaration area of size h is used. Note that the number of false alarms with declaration cannot exceed the number of false alarms with $h = 1$. Also, the maximum possible number of false alarms in a declaration area is $(h^2 - 1)$.

Proof of Proposition 1: The expected number of false alarms in a declaration area is $P_{f1}(h)(h^2 - 1)$, while the expected number of targets detected in that area is $P_{d1}(h)(h^2 - 1)$. For each of the $|N|P_{f1}(h)$ false alarms, on the average, $P_f(h^2 - 1)$ are eliminated by the effect of the declaration, since they would have been counted as false alarms with $h = 1$. However, they are not counted with an $h \times h$ declaration area. Therefore

$$|N|P_{f1}(h) \geq P_f|N| - |N|P_{f1}(h).P_f(h^2 - 1) - |T|P_{d1}(h).P_f(h^2 - 1) \quad (5)$$

where the second term on the right-hand side is the average number of false alarms that are eliminated from the false alarms with declaration, while the third term is the average number of false alarms that are eliminated by the targets detected with declaration. Dividing all terms in (5) by $|N|$, we remain with

$$P_{f1}(h) \geq P_f - P_f.P_{f1}(h)(h^2 - 1) - P_{d1}(h).P_f(h^2 - 1)\frac{|T|}{|N|}, \quad (6)$$

or

$$P_{f1}(h) \geq \frac{P_f\left[1 - P_{d1}(h).(h^2 - 1)\frac{|T|}{|N|}\right]}{1 + P_f(h^2 - 1)}. \quad (7)$$

Q.E.D.

Because $|N| \gg |T|$, the simpler approximate inequality

$$P_{f1}(h) \geq \frac{P_f}{1 + P_f.(h^2 - 1)} \quad (8)$$

can be used, which has the added advantage of not requiring knowledge of $P_{d1}(h)$.

In Fig. 3, we compare the lower bound provided by (8) with empirical false alarm probabilities obtained with various values of h for a specific set of data from [8] on the FP 20 Site. We observe that the resulting ROC curves which use the lower bounds of $P_{f1}(h)$ are, as one would expect, optimistic with respect to real data. An upper bound to the false alarm probabilities with declaration would also be quite useful.

Notice that if the false-alarm probability in the vicinity of a false alarm that has been discovered is different from P_f like a value $\hat{P}_f$ that may occur when false alarms are highly correlated spatially, then the lower-bound formula (8) becomes

$$P_{f1}(h) \geq \frac{P_f}{1 + \hat{P}_f.(h^2 - 1)}. \quad (9)$$

III. An Area-Based Detector: The δ Technique

False alarms are the major source of needless time expenditure in the search for mines. Thus, significant reductions of false-alarm rates are very valuable. In this section, we will propose and evaluate a method that significantly reduces false-alarm rates by making use of neighborhood or area information around each point visited during the search.

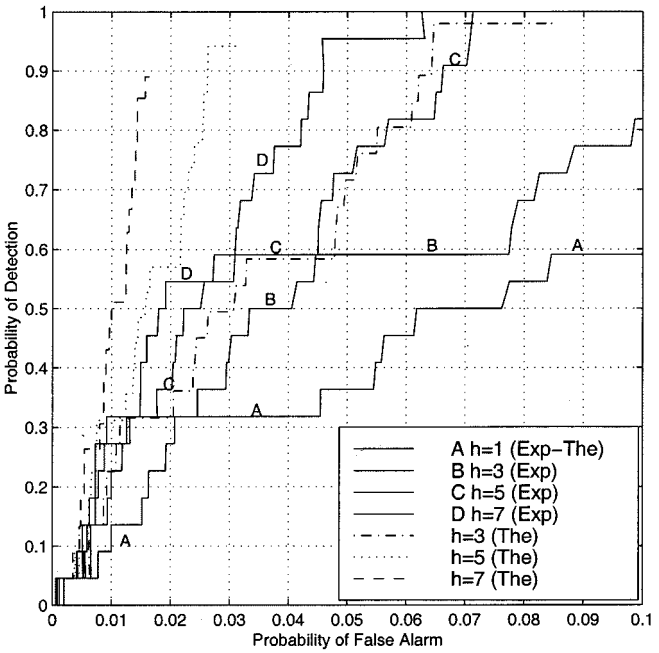

Fig. 3. Effect of declaration.

Consider again the energy measurements around two mine locations shown in Fig. 2, where we see that the energy at the mine location is higher than that at neighboring points. If this is generally true of most mine locations, and if this property were much less frequent in nontarget areas, we would hold a very good lead into a manner of reducing false alarms. In order to see whether such an idea can be fruitfully pursued, we examine the following statistic of the Z-coil data from all of the measured sites with the electromagnetic induction (EMI) sensors

$$D_n(p) = \frac{E(p) - E(p_n)}{E(p)} \quad (10)$$

where p is any point in the minefield, $E(p)$ is the EMI energy level measured by the Z-coil at point p, and $E(p_n)$ is the energy level of an immediate neighbor (there are eight of them) of the point p. $D_n(p)$ in (10) is relative to the center-point energy $E(p)$, so as to generate relative rather than absolute values. We call D_n the "local relative energ." Notice that $D_n(p) \leq 1$, but that it can take unbounded negative values. We note that $D_n(p)$ is a quantity related to some specific neighbor n of point p, so that no averaging over the eight neighbors of p is implied in (10). The local relative energy is a derived statistic we introduce, while the energy measurements themselves are available in the data from the DARPA clutter experiment. Note that each point p gives rise to eight distinct values that appear in these histograms.

Measured histograms of $D_n(p)$ for all p that are mine and nonmine locations for all available data are shown in Figs. 4–7. Also, these histograms all relate to the same set of mines that are artificially planted in them in the same relative positions and at approximately the same depth. Thus, the differences in the energy statistics of different sites are a result of the clutter and soil

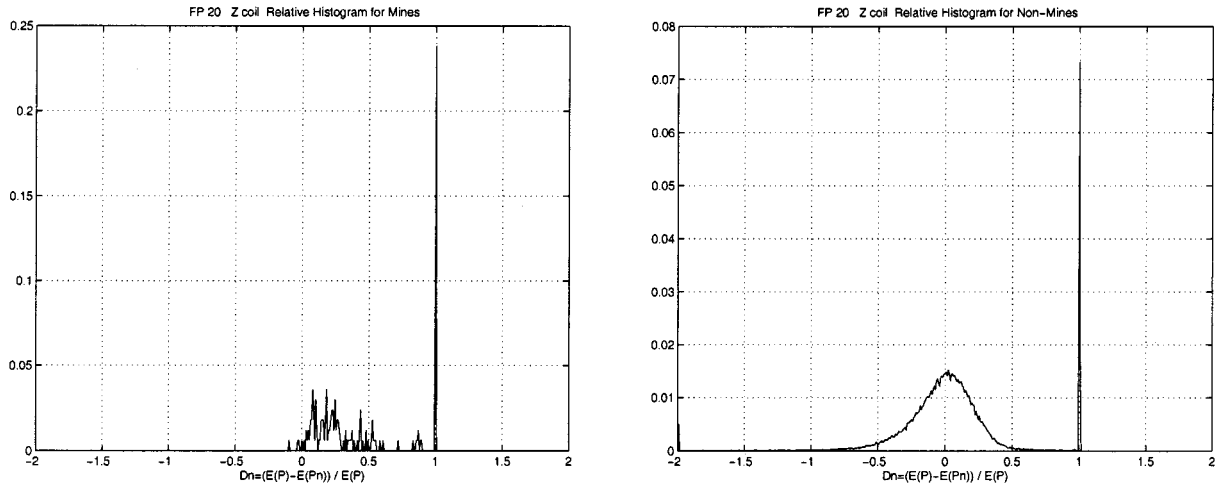

Fig. 4. Relative histogram (y-axis is the probability) of local relative energy of all mine (left) and nonmine (right) locations for FP 20.

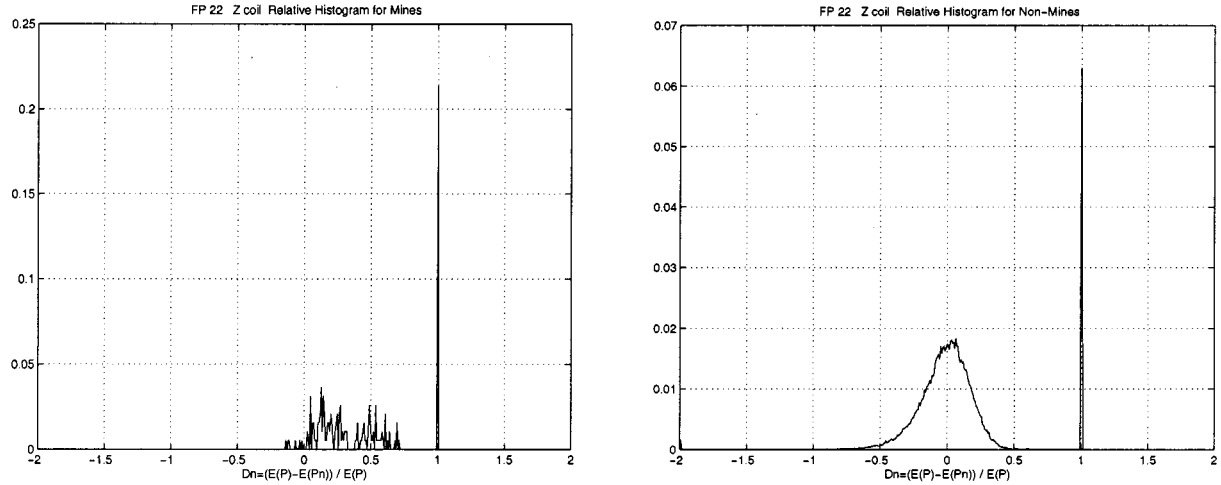

Fig. 5. Relative histogram (y-axis is the probability) of local relative energy of all mine (left) and nonmine (right) locations for FP 22.

characteristics. The clutter is a result of naturally occurring effects, as well as of various objects that may be present in the minefield without anyone's explicit knowledge. For instance, each of these areas has been actively used in the past as firing ranges, training areas, etc. Therefore, the areas will contain debris from previous usage, which will contribute in some random fashion to the clutter.

From these histograms, we always notice an accumulation point close to the value $D_n(p) = 1$, which corresponds to the case in which the neighboring points to point p exhibit very small relative energy. Other than that, we notice a very marked difference between histograms at mine locations compared to histograms at other points. At mine locations, most of the neighboring energy values are smaller than at p, so that $D_n(p)$ is positive most of the time. However, at nonmine locations, the distribution of energies is quasi-equal on either side of the energy value at p.

These observations provide us with a simple but very useful improvement on the energy detector, which we shall call the δ technique, where δ is used to denote "difference,"

1) For any selected threshold energy level θ, select all data points p where the Z-coil EMI energy $E(p) \geq \theta$. Call this set $H(\theta)$.
2) Select a number $m = 1, \cdots, 8$. For each p in $H(\theta)$, count the number of immediate neighbors P_n whose energy value is strictly less than $E(p)$, and call it $M(p)$. Notice that $M(p) \leq 8$. If $M(p) \geq m$, classify p as a mine. Otherwise, treat it as a nonmine. Clearly, many p's thus classified as mines will turn out to be false alarms.
3) We will say that $\delta = m/8$ (and in practice for many of our numerical examples we have selected $\delta = 7/8$ or $8/8$), because of the very significant clutter-rejection capabilities of these parameter settings, as shown in Fig. 8.

The effect of the δ technique on false alarms is illustrated in Fig. 8 as a function of the energy threshold θ of the detector. As the actual value of δ increases, the percentage of false alarms rejected will vary from a low value of 10% to a high value of 85%. Thus, the δ technique will significantly impact the ROC curves of an energy detector by reducing the false-alarm rates. Fig. 9 shows the ratio of false-alarm probabilities $P_f^{\delta}(h)/P_{f1}(h)$ for the two extreme cases $h = 1$ (no declaration) and $h = 7$ at the FP 20 Site, as a function of the energy threshold θ. The significant reduction in false-alarm probabilities is present even with a very large declaration area. We observe the same effect on all the other sites but

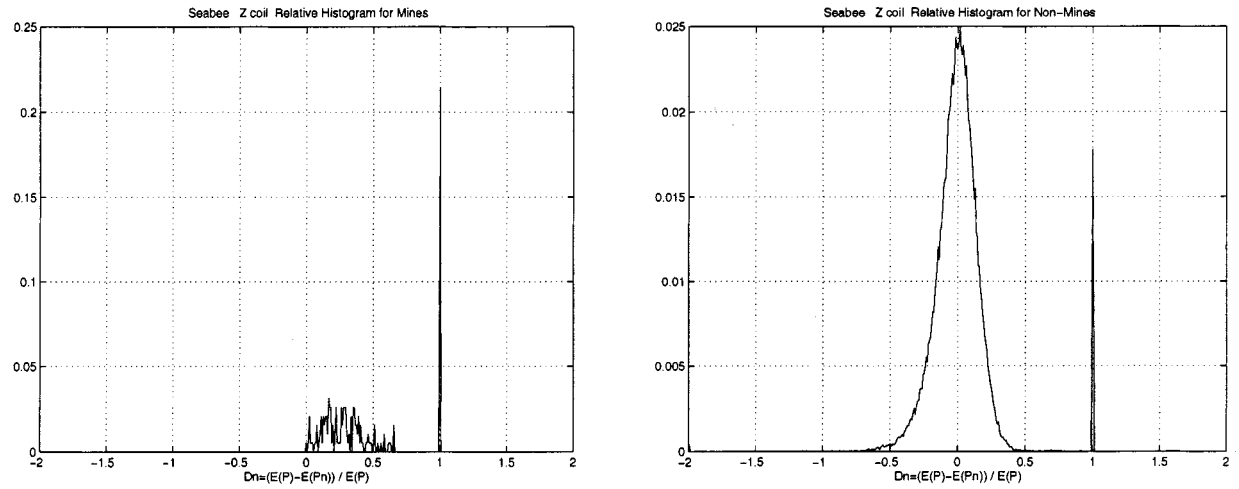

Fig. 6. Relative histogram (y-axis is the probability) of local relative energy of all mine (left) and nonmine (right) locations for Seabee.

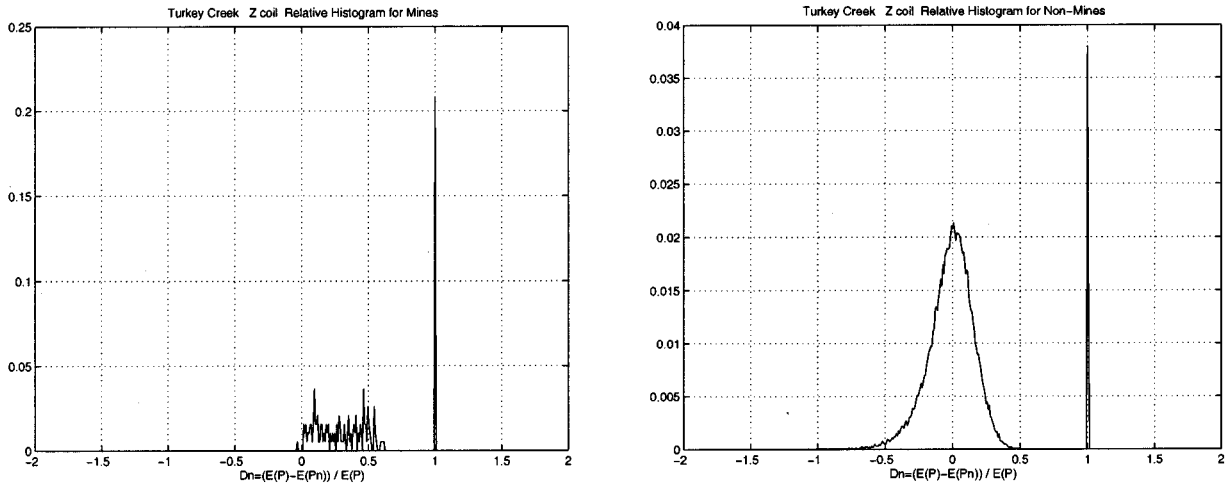

Fig. 7. Relative histogram (y-axis is the probability) of local relative energy of all mine (left) and nonmine (right) locations for Turkey Creek.

do not report all of the curves in this paper because of space limitations.

The ROC curves in Figs. 10 and 11 summarize the effect of the δ technique with $\delta = 8/8$ as compared to the simple energy detector for 1-m and 0.5-m Z-Coil data from the FP 20 Site. In these figures, the indicator "Theta" is used for the pure-energy detector. Very significant performance improvements are evident without declaration. As h increases to $h = 3$, $h = 5$ (the gain introduced by the δ technique) is still significant, but it is reduced, as seen in Figs. 12–14.

Further detailed evaluations of the δ technique are presented in Figs. 17–20, where, rather than tracing ROC curves for each different value of h, we have plotted the relative quality of the δ technique with respect to the energy detector. The measure we use in these plots is the "δ improvement ratio"

$$Q_\theta^\delta(h) = \frac{R_\theta^\delta(h)}{R_\theta(h)}. \tag{11}$$

Here, $R_{theta}^{\delta}(h)$ and $R_{theta}(h)$ are the ratios of detection to the false-alarm probability, with declaration h as a function of the energy threshold θ, with and without the δ-technique, respectively

$$R_\theta^\delta(h) = \frac{P_d^\delta(h,\theta)}{P_f^\delta(h,\theta)} \tag{12}$$

$$R_\theta(h) = \frac{P_d(h,\theta)}{P_f(h,\theta)}. \tag{13}$$

In order to illustrate the kind of improvement to be expected, on Fig. 15 we plot the ratios $R_\theta(h)$ and $R_\theta^\delta(h)$ for the FP 20 1-m Z-coil data without declaration, as a function of the energy detector's threshold. This clearly shows the improvement offered by the δ technique. On the other hand, the plot in Fig. 16 for 7×7 declaration (i.e., $h = 7$) for the same data shows that the gain to be expected from the δ technique is significantly reduced for this large value of h.

In Figs. 17–20, we present in a compact form the δimprovement ratio $Q_\theta^\delta(h)$ for all the available 1-m Z-coil data from all sites (FP 20, FP 22, Seabee, and Turkey Creek, respectively) as a function of the threshold of the energy detector θ and of the declaration h. Only threshold values for which the probability of correct detection exceeds 0.8 are con-

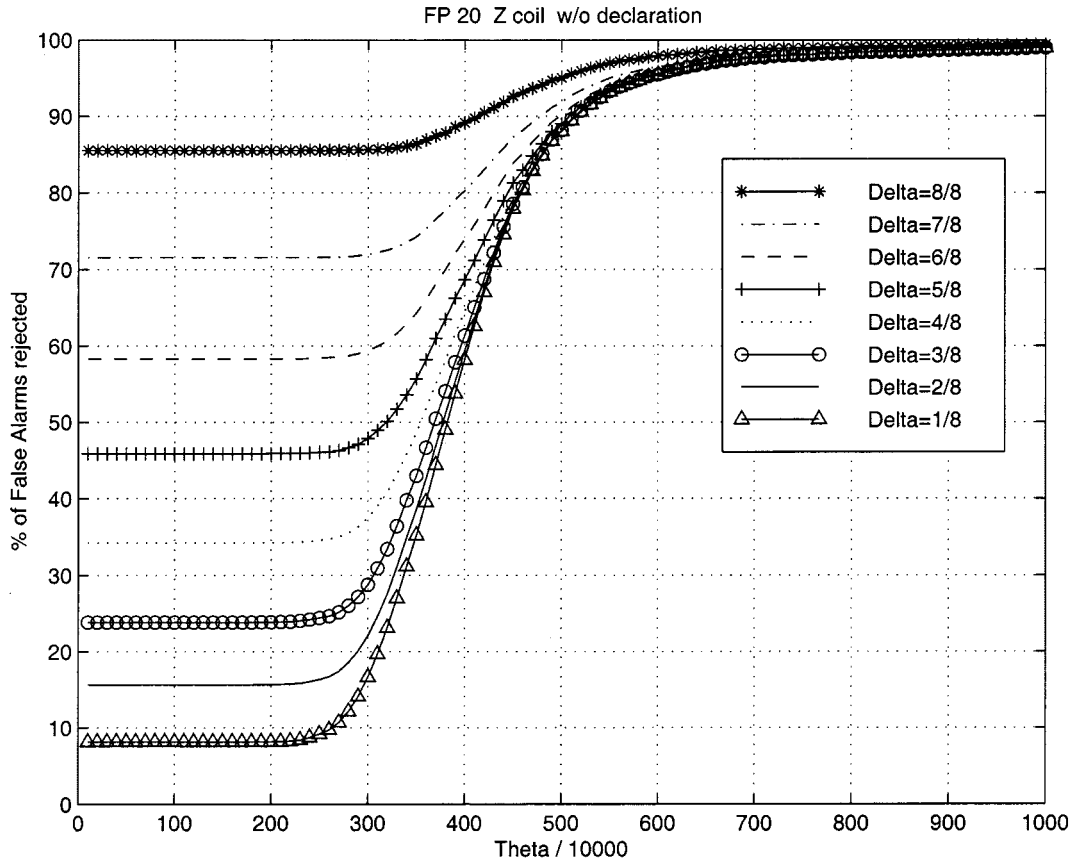

Fig. 8. Percentage of false alarms rejected, to total false alarms, with the delta technique, for values of delta running from 1/8 to 8/8. This is from raw data from FP 20 with Z-Coil 1-m measurements with $h = 1$. For this data, Theta values less than 450 correspond to a probability of correct detection higher than 0.8.

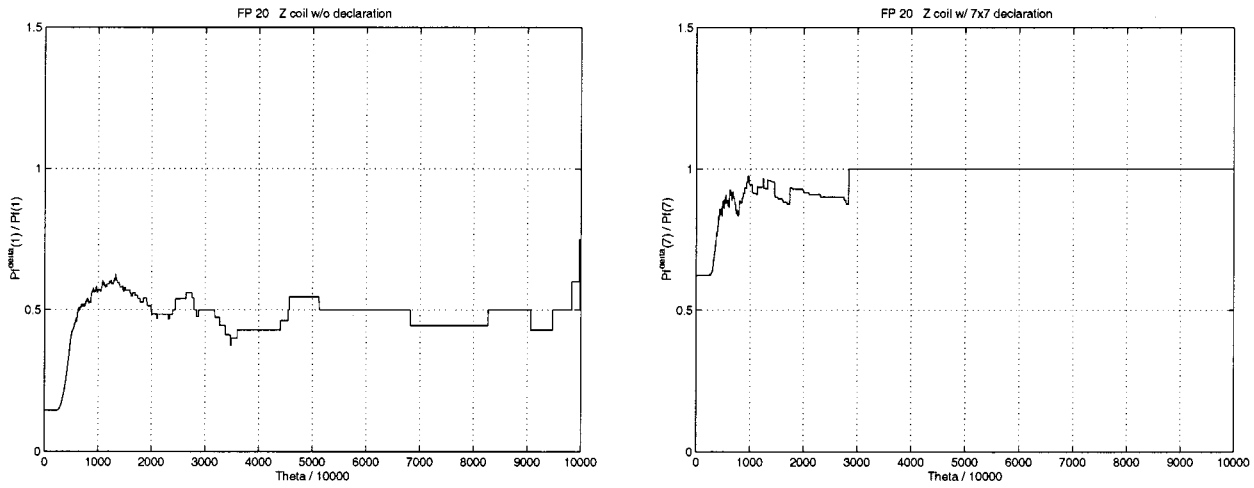

Fig. 9. Ratio of false alarm probability with the δ-technique to FA with only the energy detector for FP 20 using 1-m Z coil with $h = 1$ (left) and $h = 7$.

sidered to avoid presenting irrelevant data. We see that even for declaration areas of 7 m $\times$ 7 m, improvements are significant. For smaller values of h (1, 3, 5 m), the improvements obtained by the δ technique are indeed very significant.

A. Effect of Declaration on the δ Technique

The bounds and approximations we previously derived, which describe the effect that declaration of an $h \times h$ area will have on the receiver-operating curves, assume that decisions concerning a point are based only on the statistics at that point. However, we have just described a new detection algorithm that makes use of the shape of the energy curve at each point and in an area surrounding that point. Therefore, it is of interest to evaluate the impact of declaration in this case

Consider an algorithm that bases its decisions concerning target detection at some point p based on the fact that the energy levels in the $\Delta \times \Delta$ square centered at p are strictly lower

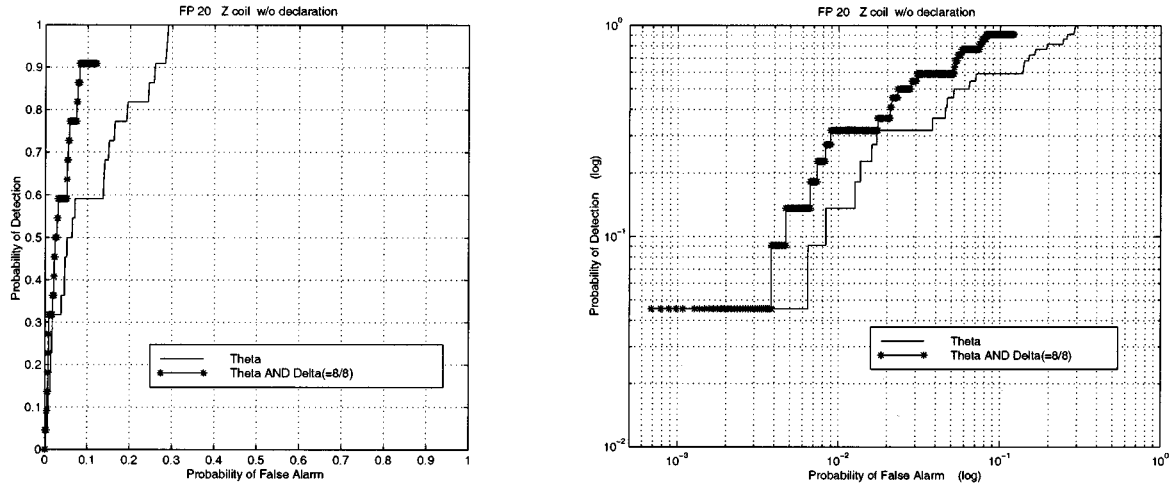

Fig. 10. ROC curves for FP 20 using the measurements of 1-m Z coil without declaration in linear and logarithmic scale.

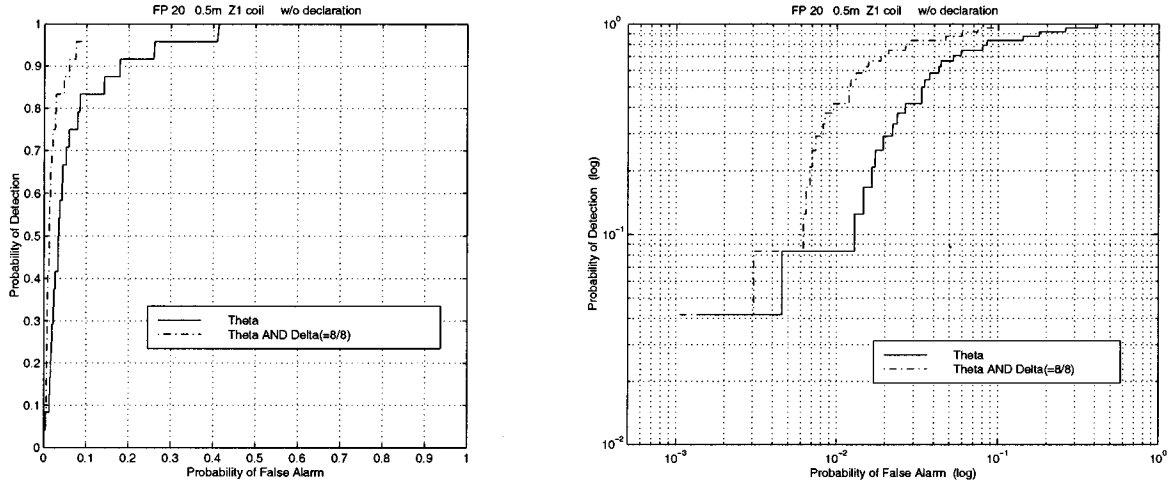

Fig. 11. ROC curves for FP 20 using the measurements of 0.5-m Z1 coil without declaration in linear and logarithmic scale.

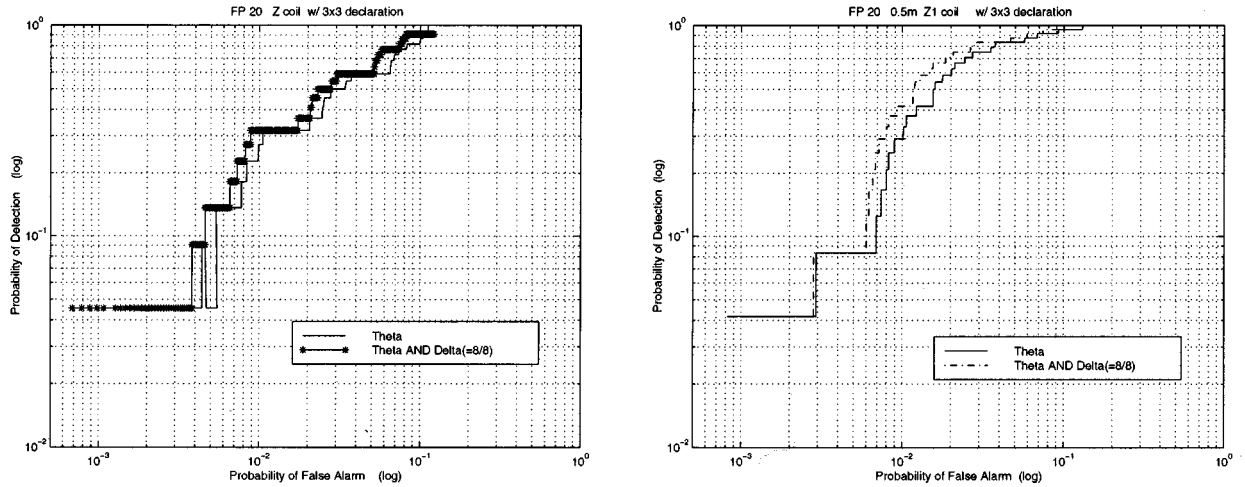

Fig. 12. ROC curves for FP 20 using the measurements of both 1-m (left) and 0.5-m (right) Z coil with 3×3 declaration in logarithmic scale.

than the energy level at p. Clearly, Δ in general needs to be an odd integer. In the results presented above for the δ technique, we have used $\Delta = 3$.

Let $h \geq \Delta$, since $h < \Delta$ is of no practical interest. Again, proceeding by means of the total number of false alarms with declaration, assuming that false-alarm rates are uniformly the

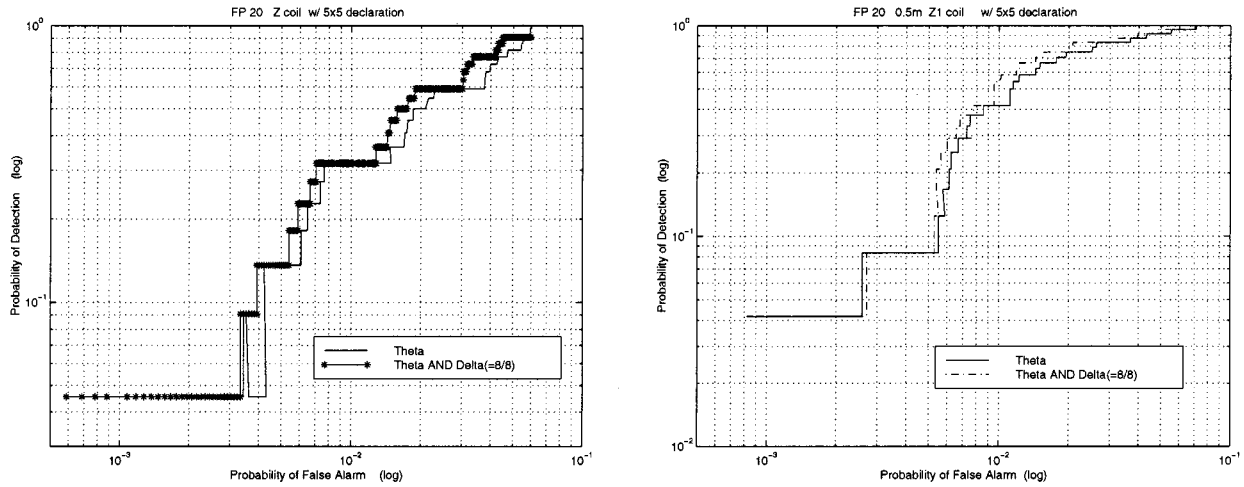

Fig. 13. ROC curves for FP 20 using the measurements of both 1-m (left) and 0.5-m (right) Z coil with 5×5 declaration in logarithmic scale.

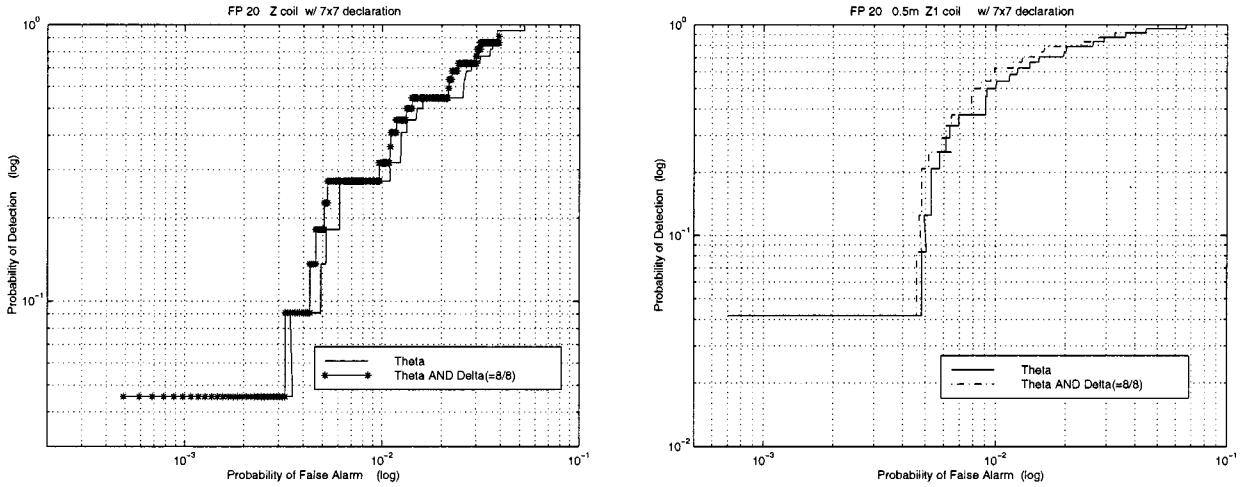

Fig. 14. ROC curves for FP 20 using the measurements of both 1-m (left) and 0.5-m (right) Z coil with 7×7 declaration in logarithmic scale.

same across the minefield (including around any detected false alarm), and using the δ technique, we have

$$P_f^\delta(h)|N| \geq P_f^\delta|N| - P_f^\delta|N|P_f^\delta(h)\left[h^2-\Delta^2\right]\frac{|N|}{|S|} - P_d^\delta(h)|T|(h^2-\Delta^2)\frac{|N|}{|S|} \tag{14}$$

where $P_f^\delta(h)$ is the probability of false alarm of the δ technique with declaration, P_f^δ is the corresponding probability without declaration, and the inequality expresses the fact that since each of the points in the $\Delta \times \Delta$-sized area around each false alarm at point p have lower energy than p, they will not in any case (with or without declaration) be considered candidates for false alarm. Thus, the saving of the number of false alarms around each point p cannot exceed $(h^2 - \Delta^2)$. This immediately leads to what is described in the following section.

Proposition 2: A lower bound for the effect of declaration on the false-alarm probability for the δ technique is given by

$$P_f^\delta(h) \geq \frac{P_f^\delta}{1+P_f^\delta(h^2-\Delta^2)}. \tag{15}$$

If false-alarm rates around detected false alarms are different (e.g., because of area-based correlations) from the average false-alarm rate across the minefield, then we can use the following inequality:

$$P_f^\delta(h) \geq \frac{P_f^\delta}{1+\hat{P}_f^\delta(h^2-\Delta^2)} \tag{16}$$

where $\hat{P}_f^\delta$ is the false-alarm rate in the immediate vicinity of a false alarm that has been discovered with the area-based detection technique.

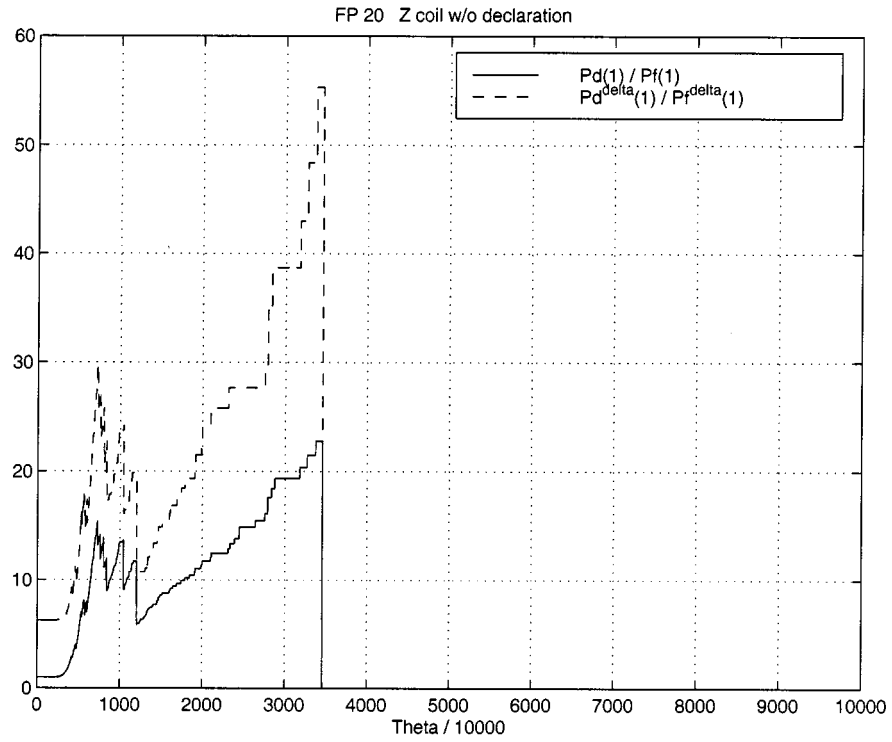

Fig. 15. Ratio of detection to false alarm probabilities for FP 20 as a function of energy detector threshold without declaration.

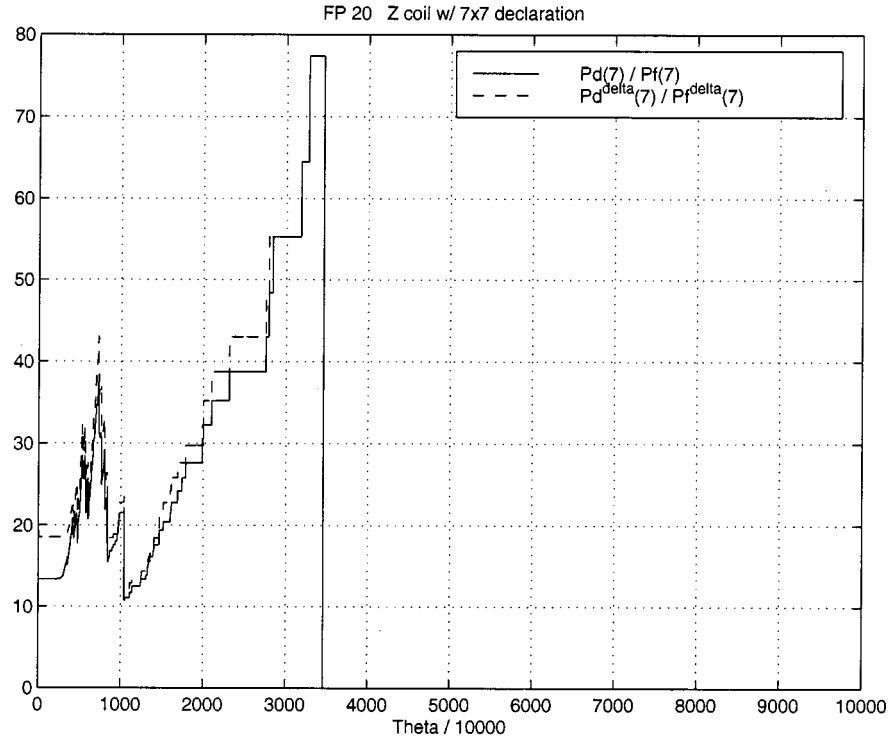

Fig. 16. Ratio of detection to false alarm probabilities for FP 20 as a function of energy detector threshold with (very large) 7-m declaration.

IV. Conclusions

In this paper, we have introduced a method called the δ technique, for reducing false-alarm rates in the detection of mines. This method can also be useful in the search for unexploded ordnance. It is based on the use of measured electromagnetic-induction energy response at and around targets.

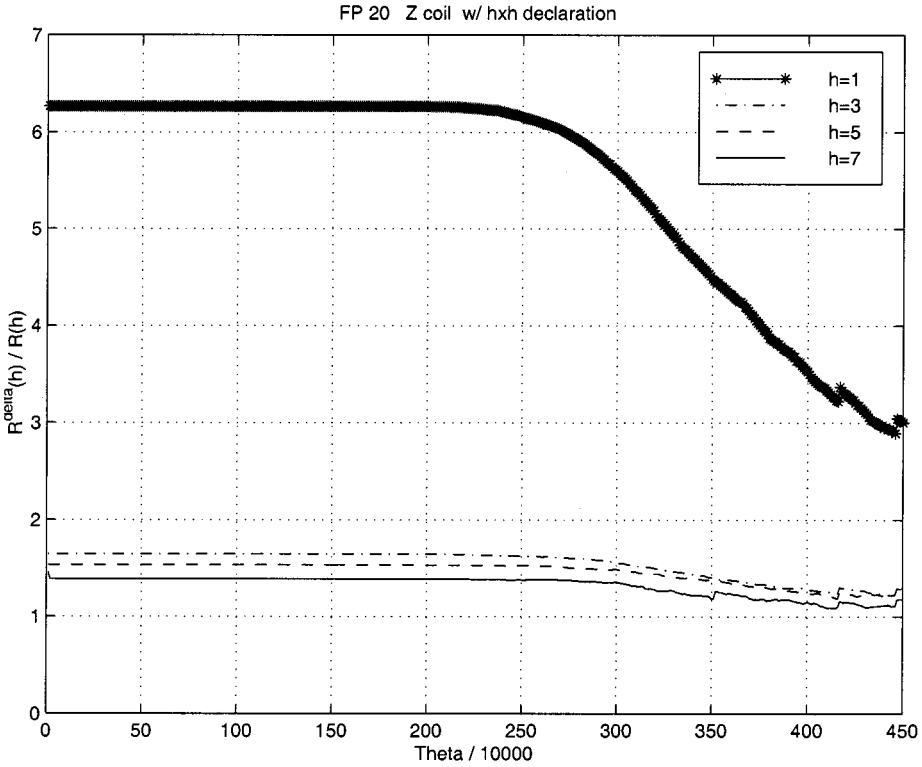

Fig. 17. Delta improvement ratio as a function of energy threshold and declaration at FP 20 Site with 1-m Z coil data.

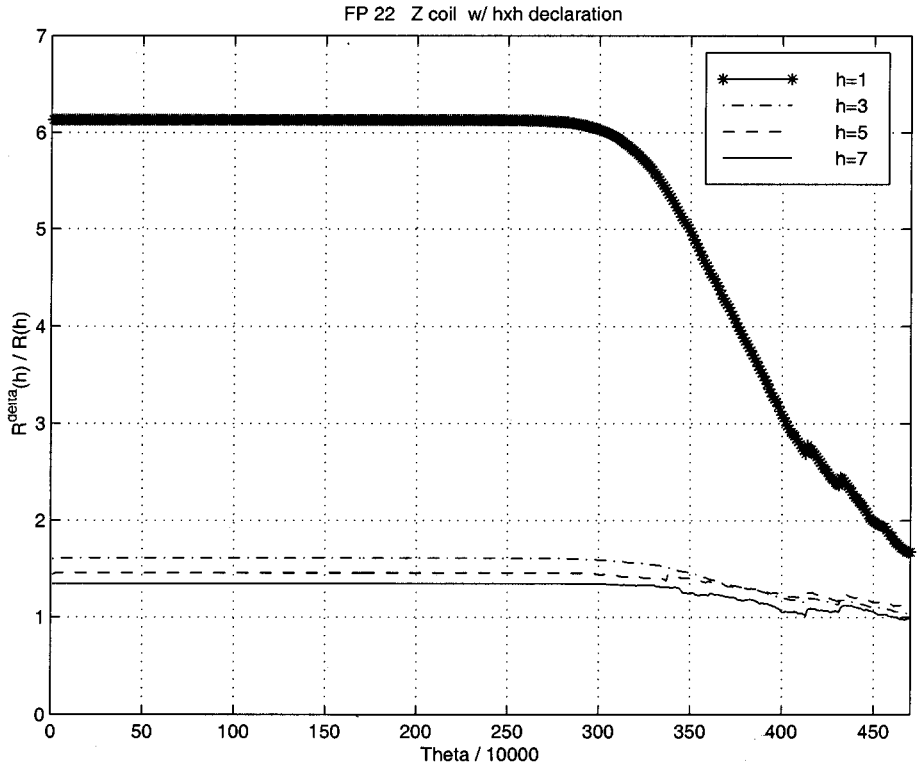

Fig. 18. Delta improvement ratio as a function of energy threshold and declaration at FP 22 Site with 1-m Z coil data.

We have also considered the effects of "declaration," which is used to take into account that immediate neighborhoods of false alarms or of detected targets should not be considered as contributing further false alarms, since they will be thoroughly examined in the process of search. A declaration area is considered to be an $h \times h$-unit area centered around the location of the target or of the false alarm [8], [10]. We derive a lower bound for false-alarm probabilities as a function of h.

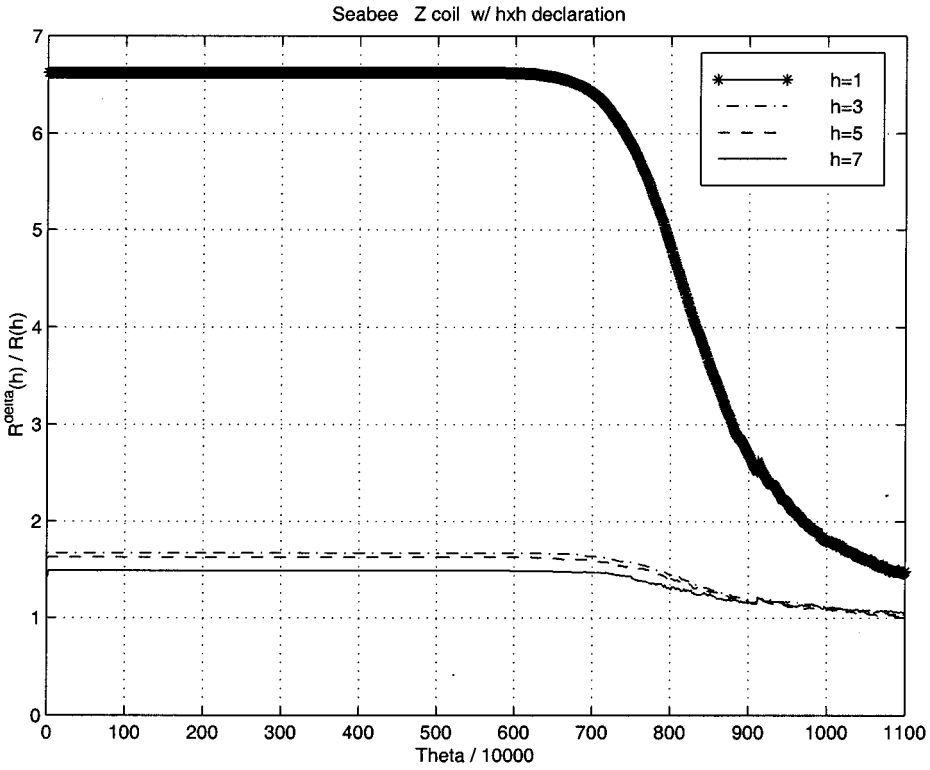

Fig. 19. Delta improvement ratio as a function of energy threshold and declaration at Seabee Site with 1-m Z coil data.

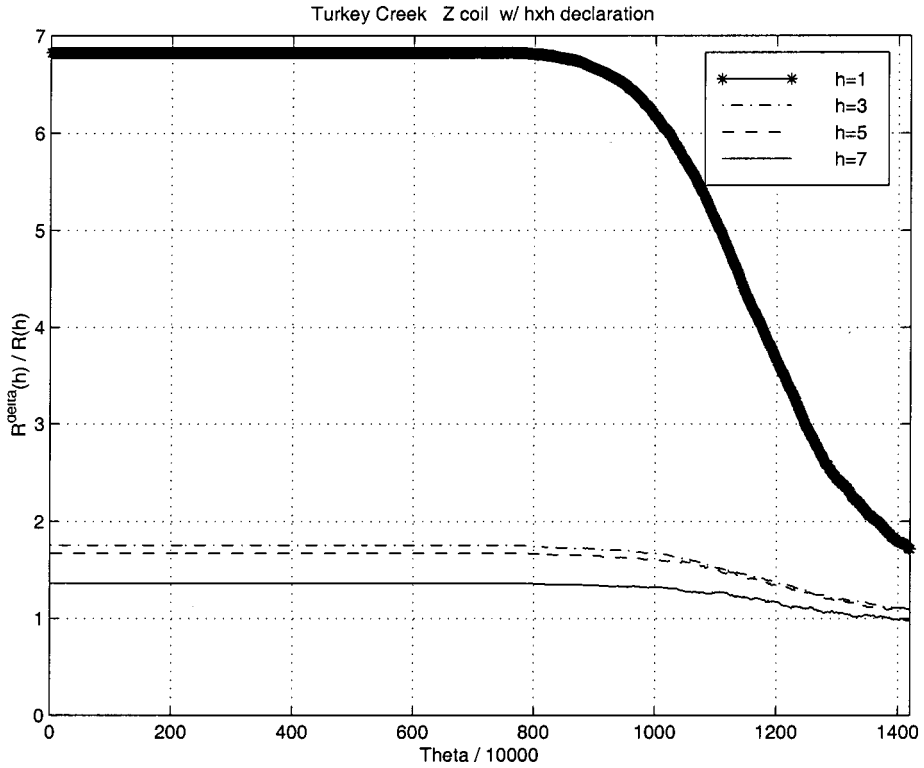

Fig. 20. Delta improvement ratio as a function of energy threshold and declaration at Turkey Creek Site with 1-m Z coil data.

We have studied the statistical distribution of energy in the immediate neighborhood of targets and of false alarms from calibrated data. The observation of specific characteristics of the difference in energy levels in the neighborhood of the two populations has led us to the δ technique. This new method considerably reduces the false-alarm rate by filtering out potential false-alarm locations whose neighbors' measured-energy levels do not have the characteristics of target neighborhoods. The reduction obtained in false-alarm rates, and the improvements in ROC curves with the δ technique, are illustrated with nu-

merous empirical results using data which has been made available through DARPA [8].

Future work will use an adaptive neural network to determine a matched filter that refines upon the δ technique. We will also fuse the approaches examined in this paper with other sensor data such as ground penetrating radar (GPR), infrared (IR), and techniques using statistical decision theory [12]. It will also be of interest to see how the δ technique can perform with other sensory data such as GPR and IR. We will also make use of the statistical data and ROC curves obtained in this paper to design efficient robotic search strategies [14].

ACKNOWLEDGMENT

The authors wish to thank R. Dugan, T. Altshuler, and V. George for providing the experimental data upon which this study is based.

REFERENCES

[1] C. R. Schwartz, A. C. Kenton, W. F. Pont, and B. J. Thelen, "Statistical parametric signature/sensor/detection model for multispectral mine target detection," *Proc. Detection Technologies for Mines and Minelike Targets*, vol. 2496, Apr. 17–21, 1995.

[2] Q. A. Holmes, C. R. Schwartz, and J. H. Seldin, "Adaptive multispectral CFAR detection of landmines," *Proc. Detection Technologies for Mines and Minelike Targets*, vol. 2496, Apr. 17–21, 1995.

[3] M. G. Bello, "A Markov random field based anomaly screening algorithm," *Proc. Detection Technologies for Mines and Minelike Targets*, vol. 2496, Apr. 17–21, 1995.

[4] M. R. Leadbetter, "Extremal methods in mine detection and classification," *Proc. Detection Technologies for Mines and Minelike Targets*, vol. 2496, Apr. 17–21, 1995.

[5] J. Glaz, "Discrete scan statistics with applications to minefield detection," *Proc. Detection and Remediation Technologies for Mines and Minelike Targets*, vol. 2765, Apr. 9–12, 1996.

[6] P. Newnham, "The use of a high spatial resolution 94 GHz radar for minefield detection," *Proc. Detection and Remediation Technologies for Mines and Minelike Targets*, vol. 2765, Apr. 9–12, 1996.

[7] R. Muise and J. A. Wright, "Coastal mine detection using the COBRA multispectral sensor," *Proc. Detection and Remediation Technologies for Mines and Minelike Targets*, vol. 2765, Apr. 9–12, 1996.

[8] V. George and T. Altschuler, "Background data collection test plan," Walcoff Associates, Tech. Rep. , Dec. 1996.

[9] J. Goutsias, "Toward a unifying optimal approach to mine detection problems," in *Proc. SPIE Conf. Detection and Remediation Technologies for Mine and Minelike Targets*, vol. 2765, Orlando, FL, Apr. 9–12, 1996, pp. 2–13.

[10] A. M. Andrews, T. W. Altshuler, V. George, and D. A. Sparrow, "Quantifying performance of mine detectors with fewer than 10 000 targets," *Proc. Detection and Remediation Technologies for Mines and Minelike Targets II*, vol. 3079, Apr. 21–24, 1997.

[11] T. Dogaru, L. Carin, B. L. Merchant, and R. Kapoor, "Electromagnetic scattering and detection of mines near a rough air-to-ground surface," *Proc. Detection and Remediation Technologies for Mines and Minelike Targets II*, vol. 3079, Apr. 21–24, 1997.

[12] L. M. Collins, T. Dogaru, L. W. Nolte, and L. Carin, "Improved decision-theoretic approach to the optimum detection of mines," *Proc. Detection and Remediation Technologies for Mines and Minelike Targets II*, vol. 3079, Apr. 21–24, 1997.

[13] R. B. Fair, M. Pollack, and V. Pamula, "MEMS trace particle, vapor and ultrasound sensor," *Proc. Detection and Remediation Technologies for Mines and Minelike Targets II*, vol. 3079, Apr. 21–24, 1997.

[14] E. Gelenbe and Y. Cao, "Autonomous search for mines," *Proc. Detection and Remediation Technologies for Mines and Minelike Targets II*, vol. 3079, Apr. 21–24, 1997.

[15] E. Gelenbe, N. Schmajuk, J. Staddon, and J. Reif, "Autonomous search by robots and animals—A survey," *Robot. Auton. Syst.*, vol. 22, pp. 23–34, 1997.

[16] T. E. Olson and C. E. Priebe, "Detection and classification of mines via discriminant features and borrowed strength," *Detection and Remediation Technologies for Mines and Minelike Targets II*, vol. 3079, Apr. 21–24, 1997.

[17] C. E. Priebe, "Exploiting stochastic partitions for minefield detection," *Detection and Remediation Technologies for Mines and Minelike Targets II*, vol. 3079, Apr. 21–24, 1997.

[18] I. V. Basawa, "Unilateral Markov random fields for minefield modeling and detection," *Detection and Remediation Technologies for Mines and Minelike Targets II*, vol. 3079, Apr. 21–24, 1997.

[19] M. M. Hayat, J. A. Gubner, and W. Chang, "Performance evaluation for detection of minefields modeled by interacting point processes," *Detection and Remediation Technologies for Mines and Minelike Targets II*, vol. 3079, Apr. 21–24, 1997.

Erol Gelenbe (S'69–M'70–SM'79–F'86) received the B.S. degree from the Middle East Technical University, Ankara, Turkey, the M.S. and Ph.D. degrees in electrical engineering from the Polytechnic Institute of Brooklyn, NY, and the D.Sc. degree in applied mathematics from the University of Paris, France.

He was the Nello L. Teer, Jr. Professor and Chair of the Electrical and Computer Engineering Department, Duke University, Durham, NC, where he held secondary appointments as a Professor of Computer Science as well as Psychology-Experimental. He is currently Professor of Computer Science and Director of the School of Electrical Engineering and Computer Science, University of Central Florida, Orlando, FL. He has authored four books and published more than 100 journal articles. He has also supervised more than 50 Ph.D. dissertations. He is Chair of the IFIP Working Group 7.3 (Computer System Modeling) and a member of the IFIP Working Group 6.4 (Performance of Computer Communication Networks). He serves on the editorial board of several journals.

Dr. Gelenbe received the IFIP Silver Core Award in 1980, the "Chevalier de l'Ordre du Merite" Award in 1992 from the French Government, the Science Award of the Parlar Foundation of Turkey in 1995, an honorary doctorate from the University of Rome in 1996, and the Grand Prix France Telecom of the French Academy of Science in 1996 for his work on stochastic networks and system performance.

Taşak Koçak (M'96) received the B.S. degree wth honors in 1996 in electrical and electronic engineering and in physics, from Bogazici University, Istanbul, Turkey, and the M.S. degree in electrical engineering from Duke University, Durham, NC, in 1998. He is currently pursuing the Ph.D. degree at Duke University.

He was a Project Engineer at Iltek High-Tech Ltd., Istanbul, from 1994 to 1996. He is currently a Technical Staff Member at Mitsubishi Semiconducter America, Inc., Durham, NC. His research interests include VLSI design, artificial neural networks, intelligent control, sensor fusion, and mine detection.

Mr. Koçak is a member of several professional societies, including the IEEE Computer, Control Systems, and Signal Processing Societies and the Turkish Informatics Society.